small methods
www.small-methods.com

Biomolecular Electron Controller Composed of Nanobiohybrid with Electrically Released Complex for Spatiotemporal Control of Neuronal Differentiation

Joungpyo Lim, Jinho Yoon, Minkyu Shin, Ki-Bum Lee, and Jeong-Woo Choi**

In vitro spatiotemporal control of cell differentiation is a critical issue in several biomedical fields such as stem cell therapy and regenerative medicine, as it enables the generation of heterogeneous tissue structures similar to those of their native counterparts. However, the simultaneous control of both spatial and temporal cell differentiation poses important challenges, and therefore no previous studies have achieved this goal. Here, the authors develop a cell differentiation biomolecular electron controller ("Biomoletron") composed of recombinant proteins, DNA, Au nanoparticles, peptides, and an electrically released complex with retinoic acid (RA) to spatiotemporally control SH-SY5Y cell differentiation. RA is only released from the Biomoletron when the complex is electrically stimulated, thus demonstrating the temporal control of SH-SY5Y cell differentiation. Furthermore, by introducing a patterned Au substrate that allows controlling the area where the Biomoletron is immobilized, spatiotemporal differentiation of the SH-SY5Y cell is successfully achieved. Therefore, the proposed Biomoletron-mediated differentiation method provides a promising strategy for spatiotemporal cell differentiation control with applications in regenerative medicine and cell therapy.

1. Introduction

Cell differentiation in living organisms is precisely regulated both spatially and temporally to form various tissues.[1–4] Numerous studies have been conducted to develop novel strategies to control cell differentiation, thus mimicking the cell differentiation patterns in living organisms.[5,6] Particularly, the spatial control of cell differentiation is critical for generating tissues with a heterogeneous structure similar to that of real tissues. Moreover, given that the time required for cells to differentiate into the desired cellular lineage varies between cells, temporal cell differentiation control is also required to modulate cell-level tissue composition at specific time points. Therefore, spatiotemporal control of cell differentiation can be applied in diverse fields such as regenerative medicine and cell therapy.[7–9]

Several studies have recently reported various strategies to control cell differentiation, including direct electrical stimulation, nanoparticle-mediated delivery of differentiation-inducing small molecules, injectable functional hydrogels, and CRISPR-Cas9-based gene editing.[10–16] However, these methods have several limitations, including nanomaterial-associated cytotoxicity, loss of cellular function due to organelle damage, and can decrease differentiation efficiency. Additionally, these methods nonspecifically induce the differentiation of all cells within a single culture plate and therefore do not allow for the spatial control of cell differentiation.[17–19] Recently, electrostimulation-based novel methods, including electropolymerized conductive scaffold, piezoelectric polymer, or magnetoelectric stimulation were reported for stem cell differentiation control. However, there is still room to be improved to demonstrate spatiotemporal differentiation control, such as the precise positioning at the cellular level using magnetic fields.[20–22]

To address these limitations, nano- or micro-pattern arrays have been developed to spatially control cell alignment and differentiation using physicochemical cues.[23,24] However, despite the many advantages of this approach, the cell types that can be differentiated through this method are primarily limited to cardiomyogenesis, osteogenesis, and chondrogenesis.[25] These properties limit the application of nano- or micro-pattern arrays for the development of comprehensive cell differentiation platforms. Moreover, cell differentiation begins as soon as the cells are seeded onto the array, and therefore physicochemical cues are not well suited to achieve temporal control of cell differentiation.[26–28] Recent studies have reported that myogenic differentiation and angiogenesis can be achieved through engineered optogenetics, thus allowing for spatiotemporal control of cell differentiation.[29] Although spatiotemporal control was achieved to some extent using light-responsive recombinant cells via the implementation of gene recombination techniques, this approach exhibited several disadvantages that hindered its

J. Lim, J. Yoon, M. Shin, J.-W. Choi
Department of Chemical & Biomolecular Engineering
Sogang University
Mapo-gu, Seoul 04107, Republic of Korea
E-mail: jwchoi@sogang.ac.kr
J. Yoon, K.-B. Lee
Department of Chemistry and Chemical Biology
Rutgers, The State University of New Jersey
Piscataway, NJ 08854, USA
E-mail: kblee@rutgers.edu
The ORCID identification number(s) for the author(s) of this article can be found under https://doi.org/10.1002/smtd.202100912.

DOI: 10.1002/smtd.202100912

practical application.[30] Concretely, given that this method must be accompanied by a gene transfection process related to the cell differentiation pathway, cell function could be negatively affected. Additionally, there would be unknown side effects associated with the transplantation of recombinant cells and it would be difficult to increase the scale of this approach to meet the demands and requirements of the medical field. Therefore, from a strictly biological standpoint, the spatiotemporal control of cell differentiation has not been reported yet.

Based on our previous findings in cell differentiation research,[31–33] biocompatible cell adhesion and cell membrane penetration are required to enable the efficient interaction between nanomaterials and cells.[34–37] Cell penetration via destructive methods such as microneedles often leads to oxidative stress, inducing structural and functional damage to the cell. Moreover, the reactive oxygen species (ROS) generated through oxidative stress inhibits the cell differentiation process, as they damage the DNA and mitochondria inside the cell. Neurons are particularly sensitive to destructive methods and ROS damage, as membrane disruption can result in neuronal death due to membrane destabilization and excitotoxicity.[38,39] Additionally, one of the key requirements of a spatiotemporal differentiation control complex is the accurate delivery of differentiation-inducing small molecules to the cells within a desired time window and region of interest.[40]

To address these issues, our study proposed a novel biomolecular electron controller (hereinafter referred to as "Biomoletron") to spatiotemporally control human neuroblastoma cell (SH-SY5Y) differentiation into dopaminergic neurons. The proposed Biomoletron is composed of recombinant azurin (rAzu), Arg–Gly–Asp tripeptide (RGD), DNA, Au nanoparticle (AuNP), a cell-penetrating peptide (CPP), and electrically released complex (ERC) modified with retinoic acid (ERC-RA) to allow for the spatiotemporal control of cell differentiation in a biocompatible manner. Because the tripeptide component of the ERC can be released via electrical stimulation, the release of RA molecules could be controlled by conjugating RA to this tripeptide.[41–45] The role of each component is as follows. First, rAzu, a part immobilized directly to the Au substrate, enables the Biomoletron to be fabricated uniformly on the Au substrate, as confirmed in our previous research.[46,47] In addition, rAzu is a type of metalloprotein that removes ROS through a redox reaction. As an intermediate connector, DNA connects rAzu and AuNP, localizes the AuNP of the Biomoletron at the intracellular region, and provides a functional group in which RGD can be introduced for attachment to the cell membrane. In the case of AuNP, during cell penetration, its excellent biocompatibility reduces the cytotoxicity compared to the other nanomaterials such as metallic oxide nanoparticles and magnetic nanoparticles,[48,49] and it provides a surface for immobilization of CPP and ERC to achieve the effective and biocompatible cell membrane penetration for the control of the release of differentiation-inducing small molecules by electrical stimulation in a temporally resolved manner.

From a structural standpoint, the Biomoletron is composed of three parts: 1) a bottom part (rAzu/single-stranded DNA [ssDNA]) for direct and efficient immobilization on the Au substrate, 2) an intermediate part (double-stranded DNA [dsDNA]/RGD) for cell adhesion and connection of the bottom part and the top part, and 3) a top part (complementary DNA/AuNP/CPP/ERC-RA) for cell penetration and induction of SH-SY5Y cell differentiation (**Figure 1**a). After seeding the SH-SY5Y cells onto the Biomoletron-modified Au substrate, the top part of the Biomoletron was located inside the cell, and temporal control of differentiation was achieved through the release of RA from the Biomoletron via electrical stimulation at a specific time. At the same time, hydrogen peroxide (H_2O_2), a type of ROS generated during half-penetration of the Biomoletron into SH-SY5Y cells, was removed by the rAzu with its redox ROS removing reaction. (Figure 1b). Moreover, by generating Biomoletron in

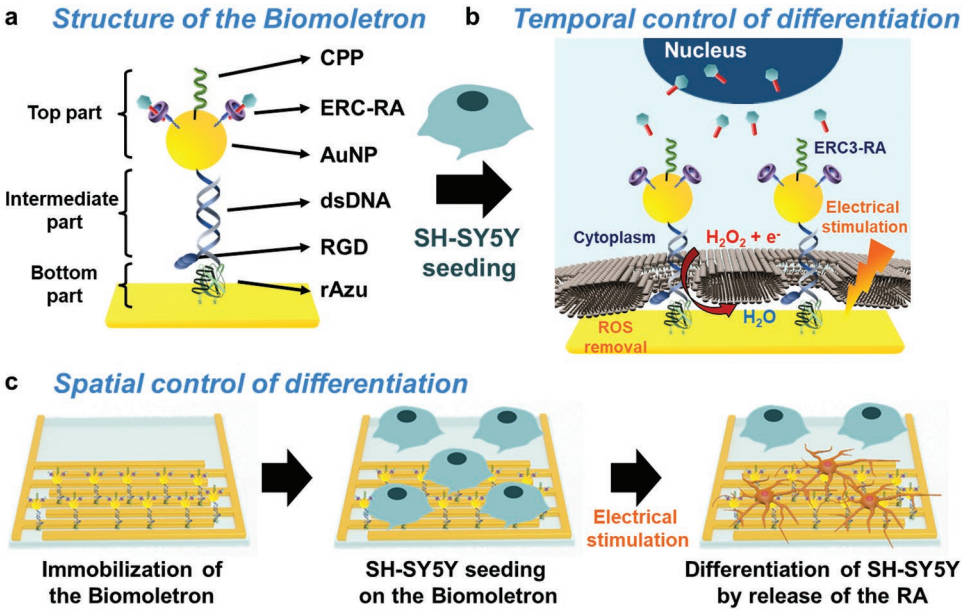

Figure 1. Design of electrically releasable Biomoletron. a) Structure of the Biomoletron. b) Temporal control of SH-SY5Y cell differentiation. c) Spatial control of SH-SY5Y cell differentiation.

certain areas of a patterned Au substrate, spatiotemporal control of SH-SY5Y cell differentiation was achieved by applying electrical stimulation to the Biomoletron at a certain time and region (Figure 1c). Collectively, the proposed Biomoletron could adhere and half-penetrate the cells with biocompatibility, thus allowing for the control of SH-SY5Ycell differentiation in a spatiotemporal manner, as a proof-of-concept study.

2. Results and Discussion

To develop the Biomoletron, the components constituting the Biomoletron must be fabricated and sequentially immobilized on the Au substrate, as shown in Figure S1, Supporting Information. We first confirmed the fabrication of the ERC via ultraviolet–visible (UV–vis) spectroscopy, after which the release of the ERC3 from the ERC via electrical stimulation was optimized through electrochemical analysis. **Figure 2**a shows the UV–vis spectra of the prepared ERC, as well as the mixture of 5,5-bis(mercaptomethyl)-2,2-bipyridine (ERC1) and the WGG tripeptide (ERC3) (ERC1+ERC3). There was no observable UV–vis peak in the ERC1+ERC3 beyond 280 nm. However, due to the formation of a ternary structure (ERC) in the presence of the cucurbit[8] uril (ERC2) with ERC1+ERC3, a UV–vis peak at 320 nm appeared upon quenching of the indole absorption through the ERC1 and ERC3 tails located in an empty space of the ERC2. A −0.5 V potential intensity was applied to the ERC, as reported in previous studies.[34] Next, in order to determine

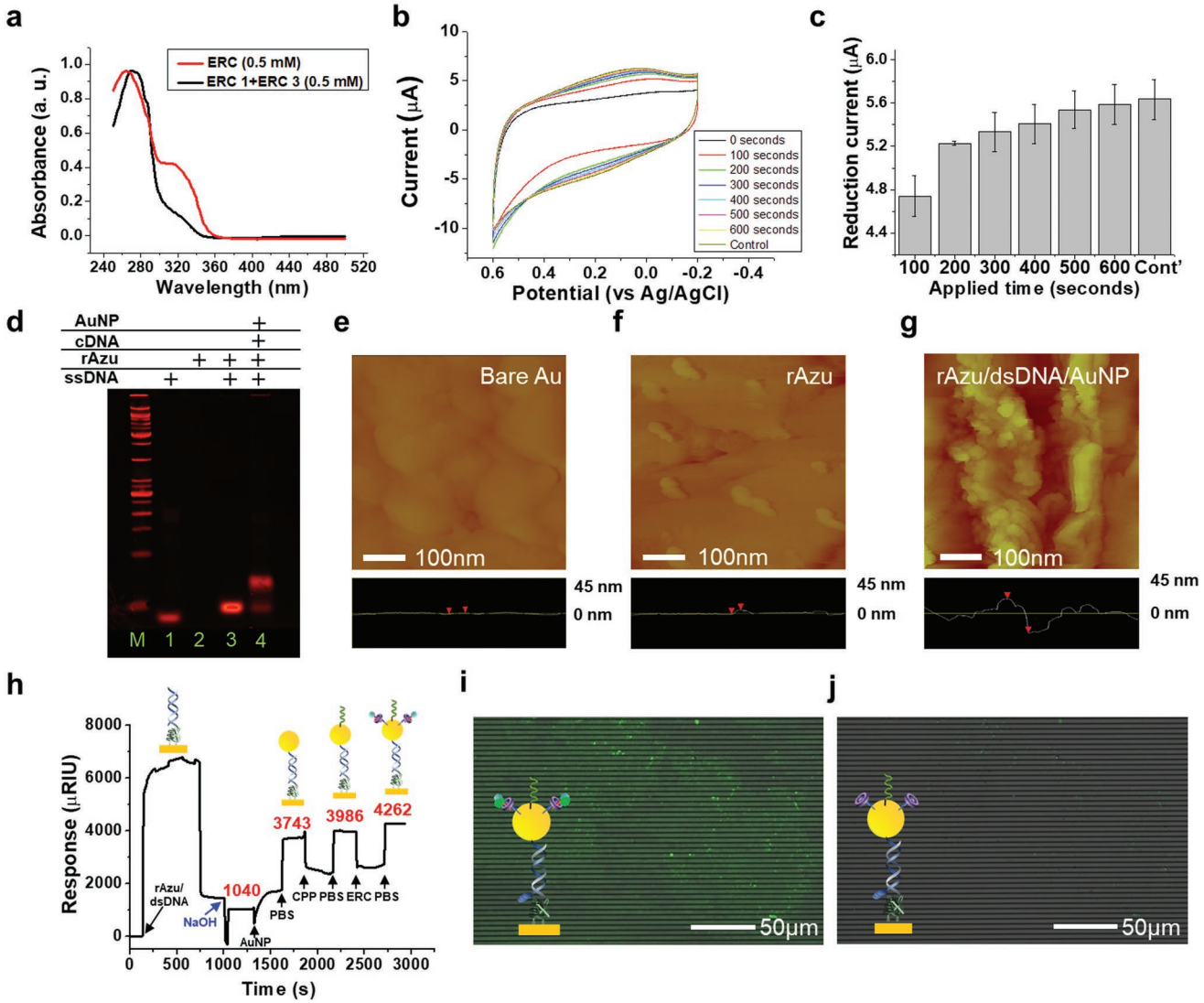

Figure 2. Development of the Biomoletron. a) UV–vis spectra of ERC and ERC1+ERC3. b) Cyclic voltammograms of the Biomoletron after electrical stimulation at 100-s intervals, and Biomoletron fabricated without the ERC3-RA (control). c) Reduction current values of the Biomoletron after electrical stimulation at 100-s intervals and Biomoletron fabricated without the ERC3-RA. d) TBE native PAGE of the ssDNA, rAzu, rAzu/ssDNA and the rAzu/dsDNA/AuNP. e–g) STM images of bare Au (e), rAzu (f), and rAzu/dsDNA/AuNP (g). h) SPR sensorgram for immobilization of the rAzu/dsDNA (ligand), with the sequential conjugation of AuNP, CPP, and the ERC (analytes) (10 mM NaOH was added at ≈1000 s to eliminate ligands that were not immobilized to the substrate). i,j) Confocal images of the Biomoletron with the ERC3/FITC, before electrical stimulation (i) and after electrical stimulation (j).

the optimal time to stimulate the ERC for the release of the ERC3, the electrochemical signals of the ERC were measured by cyclic voltammetry after electrical stimulation at different times, after which the outcomes were compared with that of the ERC prepared without ERC3 (control) (Figure 2b). As the duration of the electrical stimulation to the ERC increased at 100-s intervals, the occurrence of current reductions increased due to the release of ERC3. Moreover, when electrical stimulation was applied for 600 s, the current reduction of the ERC (9.738 μA) reached levels that were close to those of the ERC prepared without ERC3 (9.744 μA) (Figure 2c). Therefore, the optimal electrical stimulating time to the ERC was determined as 600 s.

Next, we verified the formation of the basic structure of the Biomoletron (rAzu/dsDNA/AuNP) on an Au substrate. Sequential conjugation of the rAzu, dsDNA, and the AuNP was confirmed by tris-borate-EDTA (TBE)-native polyacrylamide gel electrophoresis (PAGE). In Figure 2d, the band in lane 1 represented ssDNA, and no band was observed in lane 2 because the rAzu could not be stained by ethidium bromide. The band in lane 3 was located above lane 1, indicating that the product in lane 3 had a larger biomolecular size and weight due to the successful conjugation of the rAzu and ssDNA (rAzu/ssDNA). Similarly, the relative position of lane 4 indicated that the product increased in size and weight upon the connection of the rAzu and AuNP via dsDNA, indicating that the basic structure of the Biomoletron has been achieved. Furthermore, the immobilization of the basic structure of the Biomoletron on the Au substrate was investigated via scanning tunneling microscopy (STM). As shown in Figure 2e–g, the bare Au substrate, rAzu, and the basic structure of the Biomoletron exhibited different topography and height. Concretely, the bare Au substrate exhibited a flat surface morphology with a nearly 0.125 nm height and an ≈150 nm grain size. In the case of rAzu, the heights were ≈5 nm with an 18-nm diameter, whereas the heights for the basic structure of the Biomoletron were ≈40 nm with a 22-nm diameter. The heights of the basic structure of the Biomoletron approximately coincided with the sum of the rAzu (5 nm), dsDNA (12 nm), and AuNP (20 nm). Moreover, the diameter of the basic structure of the Biomoletron coincided with the diameter of the AuNP (20 nm) that existed at the top. These results confirmed the successful formation of the basic structure of the Biomoletron on the Au substrate. In addition, immobilization of each component on the Biomoletron was further confirmed by surface plasmon resonance through sequential layer formation (Figure 2h). The rAzu/dsDNA was first immobilized on the Au substrate as a ligand, followed by a sequential flow of analytes (AuNP, CPP, and the ERC). As the analytes became sequentially conjugated with the ligand, the response unit value increased by 2703, 243, and 276, respectively.

After confirming the successful synthesis of the Biomoletron, the electrically stimulated release of the ERC in the Biomoletron (i.e., the most important function of the Biomoletron) was monitored via fluorescent probe modification. For fluorescent verification, the fluorescein PEG amine (FITC/PEG/NH_2) was attached to the ERC3 (ERC3/FITC) instead of RA. After applying –0.5 V for 600 s to the Biomoletron modified with the ERC3/FITC, most of the ERC3/FITC were released from the Biomoletron. Figure 2i showed the FITC signals of the Biomoletron with the ERC3/FITC before electrical stimulation (indicated in green). In contrast, after electrical stimulation, the green spots largely disappeared due to the release of the ERC3/FITC from the Biomoletron at the same location (Figure 2j). In addition to these confirmation processes for the development of the Biomoletron, the fabrication process and other verification results, including CPP and RGD modification, are presented in more detail in the Figures S2 and S3, Supporting Information. Besides, we conducted the solid-state nuclear magnetic resonance analysis for the additional verification of the Biomoletron formation on the Au substrate compared to control samples prepared with bare Au substrate, and rAzu-immobilized Au substrate through the appearance of additional peaks after the Biomoletron formation (Figure S4, Supporting Information).

For efficient differentiation of SH-SY5Y cells, the Biomoletron must effectively adhere to the cellular membrane and the top part of the Biomoletron should penetrate the cells for the direct delivery of the ERC3-RA to the nucleus (Figure 1b). Two experiments were conducted using two fluorescent probes to verify the cell adhesion and half-penetration of the Biomoletron. A detailed explanation of the fabrication processes is provided in the Supporting Information.

First, to verify the cell adhesion of the Biomoletron, Texas Red maleimide (TR) was attached to the rAzu, dsDNA, and RGD conjugated complex (rAzu/dsDNA/RGD), thus forming a rAzu/dsDNA/RGD/TR complex that was then treated to the SH-SY5Y cells (**Figure 3**a). Confocal images confirmed that the rAzu/dsDNA/RGD/TR complex was effectively attached along the membrane of the SH-SY5Y cells because the RGD was connected to dsDNA (indicated in red) (Figure 3b). Next, to verify the half-penetration of the Biomoletron, a Biomoletron with a FITC/PEG/NH_2 modification instead of the ERC was fabricated on the Au substrate, after which SH-SY5Y cells were cultured for 2 days on the Biomoletron-modified Au substrate (Figure 3c). 3D confocal imaging indicated that the fluorescence signals from the FITC on the top part of the Biomoletron were located near the Hoechst-stained nucleus of the SH-SY5Y cells (indicated in blue) (Figure 3d). Although the resolution of the fluorescent analysis was not sufficient due to the limited resolution of confocal microscopy, it could be reasonably inferred that the top part of the Biomoletron successfully penetrated the SH-SY5Y cells. Taken together, these two fluorescent analyses confirmed the cell adhesion and half-penetration of the top part of the Biomoletron into the SH-SY5Y cells. Detailed information, including the fabrication process and verification of each fluorescent complex via UV–vis spectroscopy, is discussed in the Figure S5, Supporting Information. Additionally, field emission scanning electron microscopy (FE-SEM) analysis confirmed that the Biomoletrons did not decompose and remained adhered to the individual cells 7 days after the SH-SY5Y cells were seeded on the Biomoletron-modified Au substrate (Figure 3e–g).

Furthermore, the rAzu component of the Biomoletron could remove ROS that may occur during the cell penetration process due to its capacity to convert H_2O_2 to H_2O via redox reactions. H_2O_2 removal was analyzed using 2′,7′-dichlorofluorescein diacetate (DCFDA; i.e., a cell-permeant reagent). The DCFDA was deacetylated by cellular esterases into a non-fluorescent

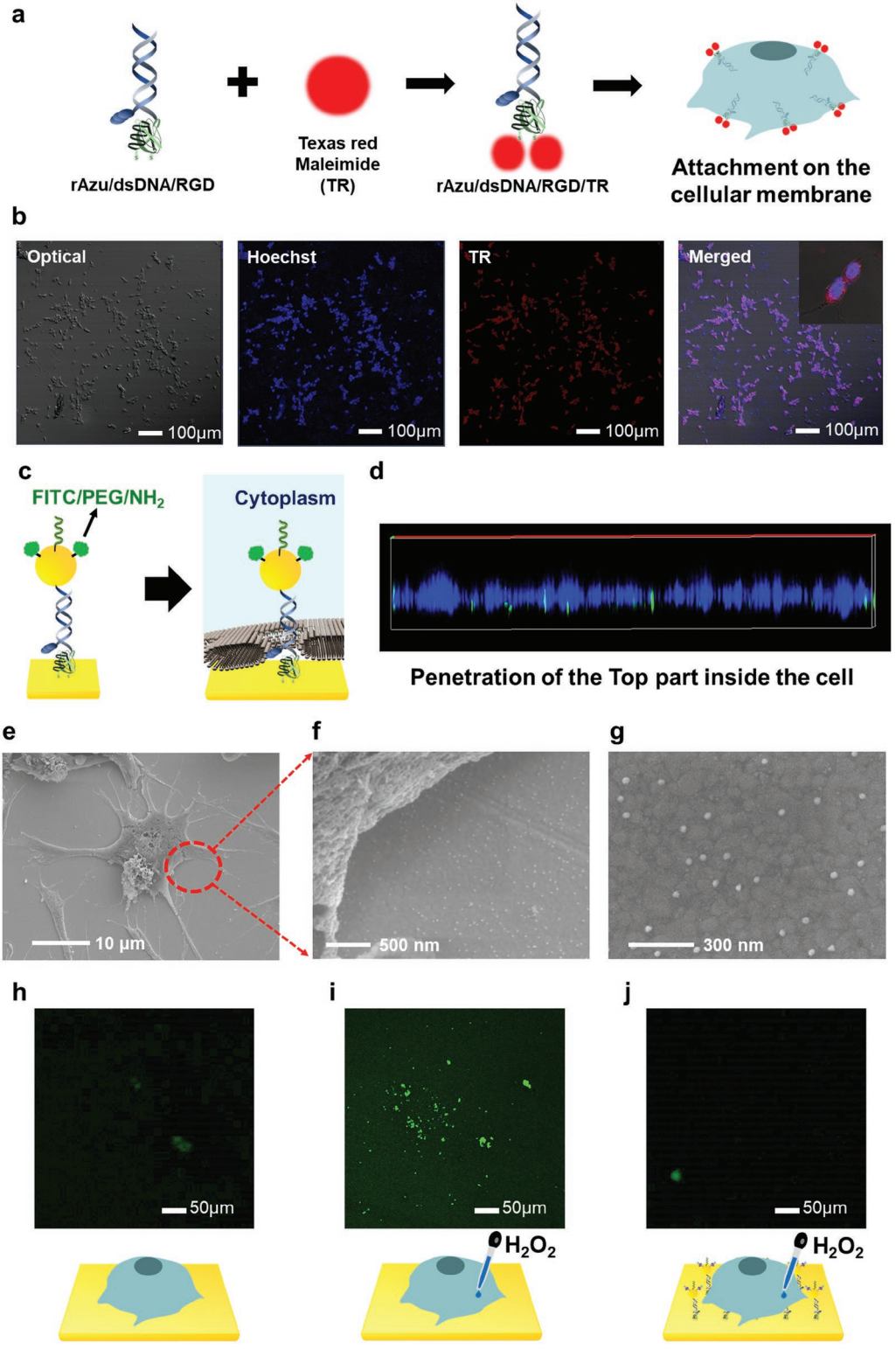

Figure 3. Adhesion and half-penetration of the Biomoletron into SH-SY5Y cell. a) Schematic images of the attachment of the rAzu/dsDNA/RGD/TR to the membrane of the SH-SY5Y cells. b) Confocal images of the SH-SY5Y cells cultured with the rAzu/dsDNA/RGD/TR for 24 h. c) Schematic image of the Biomoletron coupled with FITC/PEG/NH_2 and its cell penetration. d) 3D confocal images of the penetration of the Biomoletron with the FITC/PEG/NH_2 into the SH-SY5Y cells. e) FE-SEM images of SH-SY5Y cells on the Biomoletron immobilized Au substrate. f) Magnified image of the right edge of the SH-SY5Y cells in (e). g) Biomoletron structure immobilized near the SH-SY5Y cells, which was maintained for 7 days. h–j) Fluorescence assay for the verification of H_2O_2 removal using the DCFDA in SH-SY5Y cells cultured on the Au substrate (control) (h), H_2O_2-treated SH-SY5Y cells cultured without the Biomoletron (i), and H_2O_2-treated SH-SY5Y cells cultured with the Biomoletron (j).

compound, which is later oxidized by the H_2O_2 into 2′,7′-dichlorofluorescein (DCF), which emits a fluorescent signal. Therefore, the intensity of the fluorescent signal from the DCF is proportional to the concentration of H_2O_2.[50] As shown in Figure 3h–j, upon adding 10 μL of 1 μM H_2O_2, the SH-SY5Y cells cultured with the Biomoletron exhibited a weaker fluorescence signal compared to the controls and the SH-SY5Y cells cultured without the Biomoletron. These findings confirmed that the Biomoletron successfully removed the ROS, thus overcoming the conventional problems associated with destructive methods for cell penetration, such as neuronal death and excitotoxicity. To verify the biocompatibility of the Biomoletron, two different 3-(4,5-dimethylthiazol-2-yl)-2,5-diphenyltetrazolium bromide (MTT) assays were performed by solution and solid-state investigation (Figure S6, Supporting Information). The survival rate of SH-SY5Y cell was at least 98.17% after 24 h, and more than 98% after 48 h, proving the high biocompatibility of the Biomoletron.

The patterned Au substrate was introduced to release RA from the Biomoletron at regular intervals. Detailed information on the patterned Au substrate is discussed in the Figure S7, Supporting Information. Selective and time-dependent electrical stimulation to specific Au sections was achieved by immobilizing the Biomoletron on the patterned Au substrate. Therefore, the Biomoletron could emit RA at two different time points to effectively induce cell differentiation. Moreover, since electrical stimulation could be applied at predetermined times, temporal differentiation control of cell differentiation could be achieved by controlling the RA release time. To verify the temporal control of SH-SY5Y cell differentiation, SH-SY5Y cells were cultured on the patterned Au substrate with the Biomoletron for 7 days to fully differentiate into dopaminergic neurons by RA, which was released from the Biomoletron twice within a given time interval. As described in **Figure 4**a, SH-SY5Y cells were seeded onto the patterned Au substrate with the Biomoletron on day 0. Afterward, to induce SH-SY5Y cell differentiation, the cell culture media was exchanged only for maintenance and electrical stimulation was applied to the right Au section of the patterned Au substrate to release RA from the Biomoletron on day 1. The same electrical stimulation procedure was then repeated on day 4 to the left Au section of the patterned Au substrate. Following these steps, the time and amount of RA released from the Biomoletron could be controlled, thus allowing for effective SH-SY5Y cell differentiation.

After Biomoletron-induced cell differentiation, immunostaining was conducted to confirm the temporal differentiation of the SH-SY5Y cells (Figure 4b and Figure S8, Supporting Information). As control experiments, SH-SY5Y cell differentiation was assessed under three different conditions: case 1) the SH-SY5Y cells were cultured on the patterned Au substrate without electrical stimulation or Biomoletron; case 2) the SH-SY5Y cells were cultured on the patterned Au substrate with the Biomoletron without electrical stimulation; case 3) RA was added to the SH-SY5Y cells for differentiation without the Biomoletron (RA treatment). The other controlled conditions are presented in the Supporting Information. The conditions of the electrical stimulation to the proposed system, case S1, Supporting Information, and case S2, Supporting Information, were all the same (–0.5 V, 600 s with a 3-day interval).

For immunostaining analyses, the anti-microtubule-associated protein 2 (MAP2) and tyrosine hydroxylase (TH) were selected as markers to characterize the neuronal differentiation of SH-SY5Y cells. In case 1, normal SH-SY5Y cells maintained a small and round shape, consistent with the typical morphology of epithelial cells, and remained apart from each other without clustering. Similar morphology was also observed in case 2, as well as case S1 and case S2, Supporting Information. Moreover, only a few short neurites were identified, and no connection was observed between the adjacent cells in these cases. All of the SH-SY5Y cells cultured under these conditions exhibited the morphological characteristics of undifferentiated cells. In contrast, in case 3, SH-SY5Y cells exhibited distinct morphological features such as an elongated shape. Additionally, the SH-SY5Y cells tended to aggregate to form clusters. These morphological changes were also observed in the proposed system. Furthermore, several connections between adjacent SH-SY5Y cells by extension of the neurites were observed in both cases. Particularly, TH expression was only observed in case 3 and the proposed system, and it was thus confirmed that the SH-SY5Y cells successfully differentiated into dopaminergic neurons upon coupling Biomoletron with electrical stimulation. Moreover, quantitative PCR analysis was conducted to more precisely characterize the messenger RNA (mRNA) expression levels of the synapse-associated protein 97 (SAP 97) and the neuron-specific enolase (NSE) (Figure 4c,d). In the case of the SH-SY5Y cells differentiated via Biomoletron, the mRNA expression levels of the SAP 97 and NSE genes increased remarkably by 1.97- and 6.07-fold compared to undifferentiated SH-SY5Y cells (control) and reached even higher levels than those obtained via direct RA exposure (RA treatment). Moreover, reverse-transcription polymerase chain reaction was conducted to determine the expression of several neuronal mRNA markers (Figure 4e). Compared to the controls, the mRNA expression levels of the MAP2, synapsin (SYNS), dopamine active transporter (DAT), TH, neurofilament (NF), and NSE genes upon Biomoletron treatment were substantially higher. In addition, to verify the temporal differentiation control property of the Biomoletron more clearly, after seeding of SH-SY5Y cells on the Biomoletron-immobilized Au substrates at the same time, the initiation time of differentiation was controlled based on two different schedules with the first electrical stimulation on Day 1 and the second stimulation on Day 4 for one sample, and the first stimulation on Day 3 and the second stimulation on Day 6 for the other sample. The time interval between the first and the second electrical stimulation was the same in both samples. From the results, we confirmed that the fully differentiated time point was successfully regulated in a temporally resolved manner by the Biomoletron depending on the initiation time (Day 7 for the first sample, and Day 9 for the second sample) (Figure S9, Supporting Information). Based on these results, the temporal control of SH-SY5Y cell differentiation using the Biomoletron was successfully demonstrated.

Beyond temporal differentiation control, we next sought to assess whether the proposed Biomoletron could spatiotemporally control cell differentiation in combination with patterned

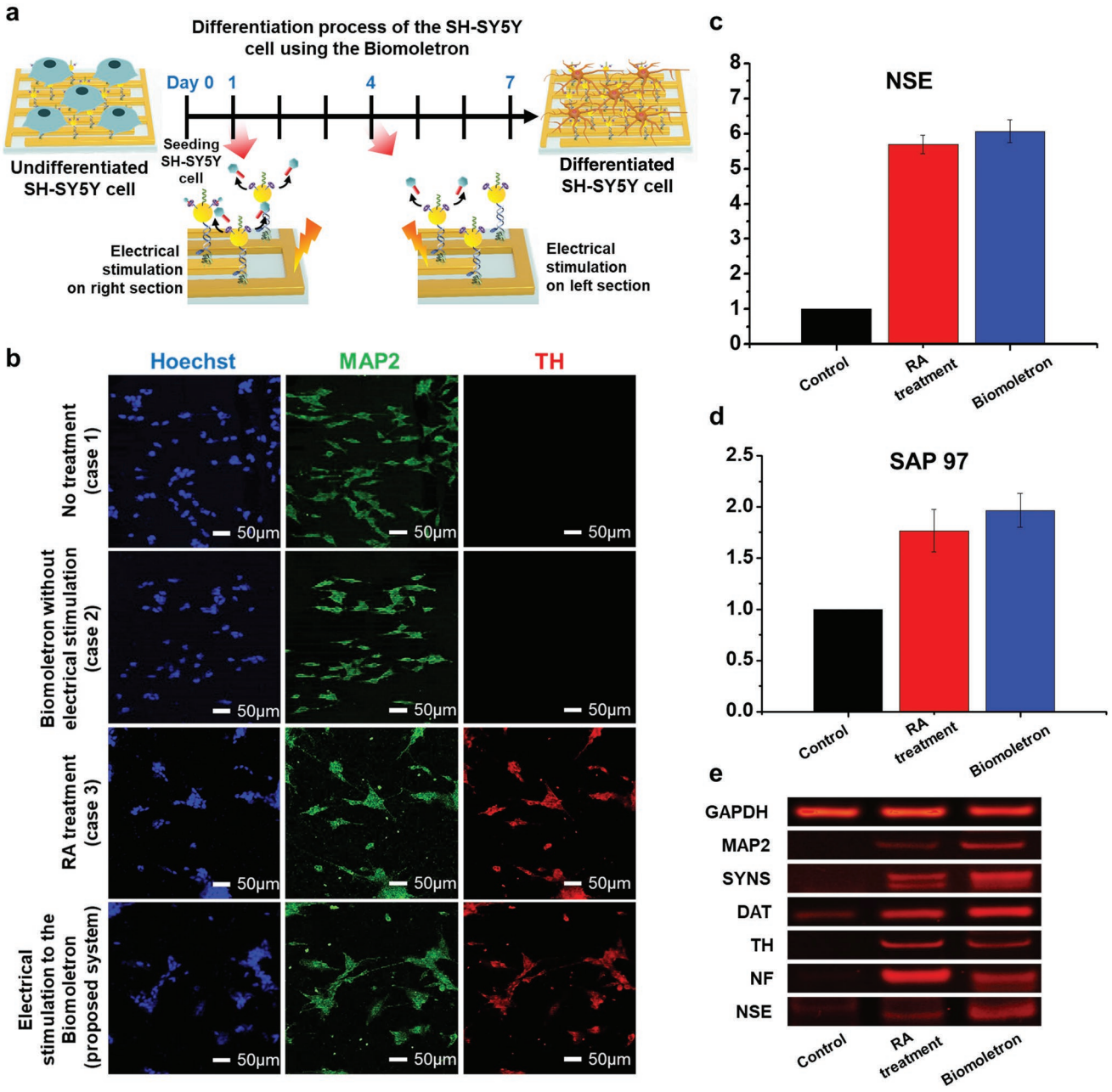

Figure 4. Temporal control of SH-SY5Y cell differentiation using the Biomoletron. a) Schematic image of the 7-day differentiation process of SH-SY5Y cells using the Biomoletron. b) (From top to bottom) Confocal images of SH-SY5Y cells cultured with no treatment (case 1), Biomoletron without electrical stimulation (case 2), RA treatment (case 3), and electrical stimulation to the Biomoletron (proposed system). c,d) qPCR analysis of the SH-SY5Y cells with the neuronal markers of SAP 97 (c) and NSE (d). e) RT-PCR analysis of the neuronal markers including MAP2, SYNS, DAT, TH, NF, and NSE.

Au substrates. This was achieved through the selective immobilization of the Biomoletron in certain areas in which the cells were seeded. As illustrated in **Figure 5**a, the Biomoletron was exclusively immobilized on the Au patterned area and the SH-SY5Y cells were seeded on the substrate areas, after which spatiotemporal control was demonstrated by the selective induction of SH-SY5Y cell differentiation only on the Biomoletron-modified region. As shown in Figure 5b, the patterned Au substrate was composed of two different regions (i.e., a glass area and an Au patterned area) where the Au line and glass line intersected, and these regions were divided by a horizontal line in the center. On this patterned Au substrate, the Biomoletron was immobilized only on the Au patterned area via Au—thiol bonding, and the selective Biomoletron immobilization was confirmed by FE-SEM characterization. Figure 5c showed the bare Au patterned area before the Biomoletron immobilization. In contrast, after Biomoletron immobilization, the Biomoletron was located only on the Au pattern line and not on the glass region (Figure 5d). Afterward, the SH-SY5Y cells were seeded on the whole surface of the pattered

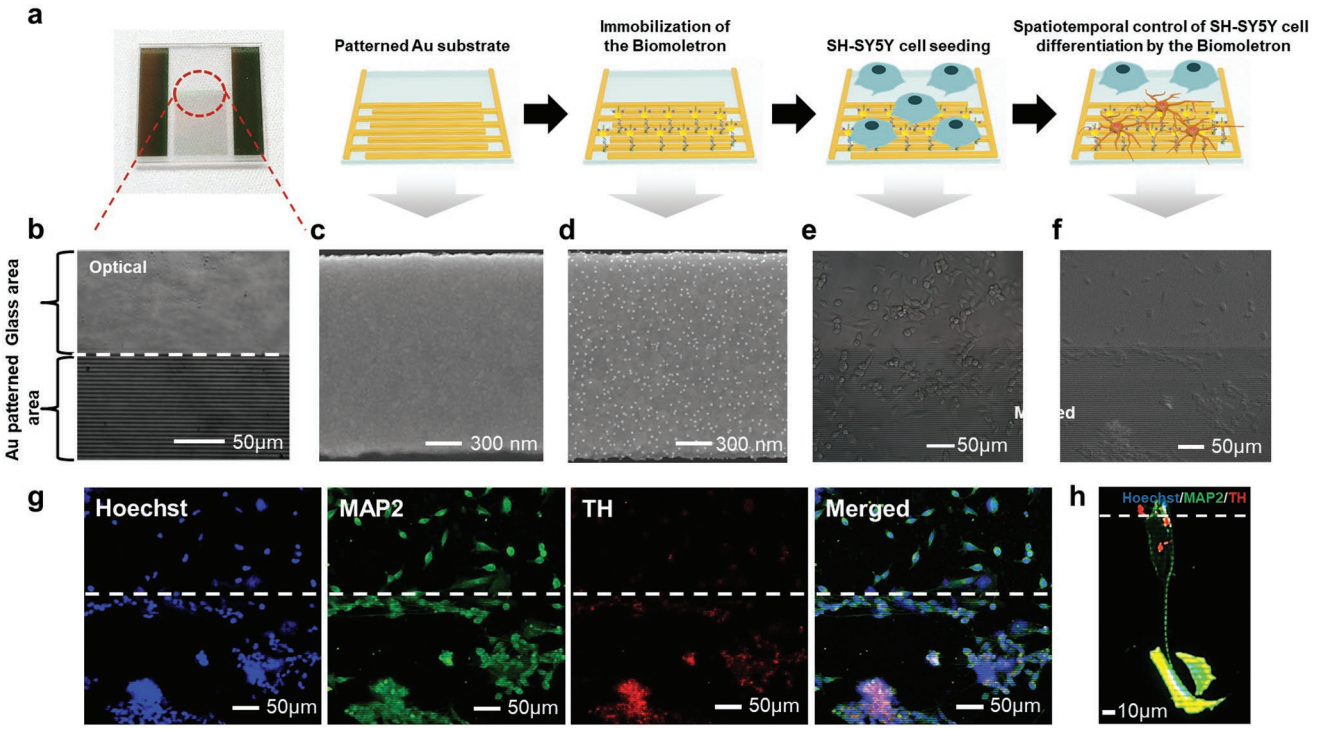

Figure 5. Spatiotemporal control of SH-SY5Y cell differentiation using the Biomoletron. a) Spatiotemporal differentiation process of SH-SY5Y cells using the Biomoletron. b) Optical images of patterned Au substrate. FE-SEM images of the Au patterned area c) before and d) after immobilization of the Biomoletron. e,f) Optical images of SH-SY5Y cells seeded on the Biomoletron-immobilized patterned Au substrate after 1 day (e) and 7 days with electrical stimulation (f). g,h) Confocal images of spatiotemporally differentiated SH-SY5Y cells on the patterned Au substrate. The area above the white dotted line represents the glass area and the lower part is the Au patterned area.

Au substrate, including the glass area and Au patterned area (Figure 5e). Next, cell differentiation was induced under the same electrical stimulation conditions as in the temporal differentiation control.

The spatiotemporal control of SH-SY5Y cell differentiation using the Biomoletron immobilized on specific areas was confirmed by optical (Figure 5f) and confocal imaging (Figure 5g). Besides, to confirm the effect of the Biomoletron-immobilized patterned Au substrate for spatiotemporal differentiation, we performed the control experiment that SH-SY5Y cells were seeded on the patterned Au substrate modified with the Biomoletron and monitored its differentiation states applying no electrical stimulation (Figure S10, Supporting Information). Similar to the results of the temporal differentiation control, undifferentiated SH-SY5Y cells remained as separate single cells on the upper half of the substrate, in which the Biomoletron was not immobilized. In contrast, differentiated SH-SY5Y cells formed cell clusters in the lower half of the substrate, where the Biomoletron was immobilized, as they differentiated into the neuron (Figure 5f). To confirm the differentiation of the SH-SY5Y cells, the MAP2 and TH genes were selected as neuronal differentiation markers and SH-SY5Y cells were analyzed by immunostaining following the same procedures as with the temporal differentiation experiments. As shown in Figure 5g, TH (i.e., a dopaminergic neuronal differentiation marker) expression was clearly observed in the lower half. In contrast, no clear TH expression was observed in the upper half, indicating that the cells remained undifferentiated. Although it was difficult to clearly observe whether the neurite stretched out of the clusters because of the only introduction of RA for inducing SH-SY5Y differentiation without changing other culture conditions, the well-formation of clusters were distinctly seen, and the neurite of differentiated SH-SY5Y was obtained as shown in zoomed-in image of Figure 5h and full image in Figure S10a, Supporting Information. Besides, the expression of TH could be easily appreciated on the lower half compared to the upper half, thus confirming the spatiotemporal control of SH-SY5Y cell differentiation into dopaminergic neurons. Furthermore, as shown in Figure S10a,b, Supporting Information, it was confirmed that some SH-SY5Y cells on the Biomoletron immobilized patterned Au substrate were differentiated, and the formation of clusters and neurites was observed. Besides, as shown in the control experiment (Figure S10c, Supporting Information), SH-SY5Y cells, which were seeded on the patterned Au substrate modified with the Biomoletron but without any electrical stimulation, remained separated single cells on the whole surface as same with the undifferentiated cells, which verified that the patterned Au substrate modified with the Biomoletron is suitable for spatiotemporal differentiation control. Taken together, these results demonstrated that the Biomoletron could be applied to control the spatiotemporal differentiation of cells. However, further studies are required to optimize the fabrication of designed patterns for the simultaneous spatial differentiation control of multiple cells, the introduction of various types of differentiation-inducing small molecules on the

Biomoletron, and the establishment of optimal conditions for Biomoletron fabrication. These efforts may enhance the spatiotemporal control of cell differentiation in multiple cellular lineages simultaneously, thus opening new avenues for the development of cell manipulation techniques with potential applicability in regenerative medicine and cell therapy.

As described in Figure S11a, Supporting Information, the human brain consists of three main cell types, including neurons, oligodendrocytes, and astrocytes, in addition to various types of subcells that populate each part of the brain.[51] The Biomoletron can conjugate not only with RA to induce cell differentiation into neurons but also with other types of differentiation-inducing small molecules for the generation of different cell types such as oligodendrocytes and astrocytes. Therefore, the reproduction of brain tissues composed of multiple brain cell types on a single chip could be achieved by designing chip patterns and adjusting the arrangement of the Biomoletron as depicted in Figure S11b, Supporting Information. Moreover, when considering the differences in the times required for cells to fully differentiate into each desired cellular lineage, the temporal differentiation technique proposed herein allows the cells to complete their differentiation process at the same time by varying the times at which the electrical stimuli are applied to the cells to induce astrocytogenesis (30 differentiation days), oligodendrogenesis (25 differentiation days), and neurogenesis (7 differentiation days).[52,53]

3. Conclusion

Spatiotemporal control of cell differentiation is essential for the in vitro reproduction of realistic heterogeneous tissue structures for biomedical applications. However, no studies had thus far achieved this goal due to its many inherent challenges. In this study, as a proof-of-concept study, we demonstrated the spatiotemporal control of SH-SY5Y cell differentiation into dopaminergic neurons for the first time using the Biomoletron. The proposed Biomoletron is composed of rAzu, RGD, DNA, AuNP, CPP, and ERC-RA, and is capable of releasing differentiation-inducing small molecules via electrical stimulation at specific times and in predetermined regions of a patterned Au substrate. The rAzu and AuNP components of the Biomoletron were used to directly and efficiently immobilize the Biomoletron on the substrate to gain access to the surface located within the SH-SY5Y cells for CPP and ERC-RA modification. dsDNA was used to connect the top and bottom parts, as well as for RGD modification. Due to the introduction of CPP and RGD, the Biomoletron successfully adhered to and half-penetrated the SH-SY5Y cells. Moreover, the release of RA to induce SH-SY5Y cell differentiation was controlled by the ERC component of the Biomoletron via electrical stimulation, thus achieving spatiotemporal control of differentiation. The temporal control of cell differentiation using the Biomoletron was conducted by applying a −0.5 V electrical stimulus to the Biomoletron on the patterned Au substrate at 3-day intervals. This triggered the release of RA from the Biomoletron, thus inducing the differentiation of SH-SY5Y cells into dopaminergic neurons within 7 days. By sequentially applying electrical stimulation to each Biomoletron immobilized on the independent Au section of the patterned Au substrate at 3-day intervals, the amount of RA released from the Biomoletron could be precisely regulated. Compared to undifferentiated SH-SY5Y cells, the expression levels of SAP97 and NSE (i.e., two representative neuronal differentiation markers) were significantly increased by 1.97 and 6.07 times, respectively, in differentiated SH-SY5Y cells treated with the proposed Biomoletron. Additionally, the H_2O_2 generated by the half-penetration of the Biomoletron into the cells was successfully removed via the ROS-removing properties of rAzu. Moreover, spatiotemporal control of SH-SY5Y cell differentiation was successfully demonstrated by selective immobilization of the Biomoletron on a certain area of a patterned Au substrate, thus achieving spatial control of RA release. When electrical stimulation (−0.5 V, 3-day interval) was applied, only SH-SY5Y cells in the Biomoletron immobilized region were selectively differentiated into dopaminergic neurons, whereas the cells remained undifferentiated when they were untreated. Taken together, our results demonstrate that the proposed Biomoletron can successfully control the differentiation of SH-SY5Ycells into dopaminergic neurons in a spatiotemporal manner when coupled with a patterned Au substrate.

Nevertheless, several issues must be further assessed, including optimizing the concentration and ratio of the Biomoletron components and introduction of the other differentiation-inducing small molecules for inducing the SH-SY5Y differentiation with distinct formation of neurites, determining the optimal time points for the application of electrical stimuli, and the design of chips allowing for the implementation of various types of Biomoletron modified with different differentiation-inducing small molecules and that can be placed precisely in the desired location. Through these additional studies, the proposed Biomoletron will enable scientists to generate various kinds of heterogeneous tissue structures composed of multiple cell types. Moreover, by scaling up the Biomoletron-modified substrate with various differentiation-inducing small molecules, the proposed Biomoletron will be applicable to commercial medical applications, thus allowing for the mass-production of various types of desired functional cells. By addressing these issues, the proposed Biomoletron-mediated novel differentiation method provides a promising strategy for spatiotemporal cell differentiation control with potential applications in regenerative medicine and cell therapy.

Supporting Information

Supporting Information is available from the Wiley Online Library or from the author.

Acknowledgements

J.L. and J.Y. contributed equally to this work. This work was supported by the National Research Foundation of Korea (NRF) grant funded by the Korea government (MSIT) (No. 2019R1A2C3002300), by National R&D Program through the National Research Foundation of Korea (NRF) funded by Ministry of Science and ICT

(NRF-2021M3H4A1A01079399), and Samsung Research Center Funding for Future Research.

Conflict of interest

The authors declare no conflict of interest.

Data Availability Statement

Research data are not shared.

Keywords

biomolecular electron controllers, biomoletrons, cell differentiation, cell therapy, regenerative medicine, spatiotemporal differentiation control

Received: August 10, 2021
Revised: November 11, 2021
Published online:

[1] D. Álvarez-Errico, R. Vento-Tormo, M. Sieweke, E. Ballestar, *Nat. Rev. Immunol.* **2015**, *15*, 7.
[2] A. J. Merrell, B. Z. Stanger, *Nat. Rev. Mol. Cell Biol.* **2016**, *17*, 413.
[3] H. N. Lee, Y. Y. Choi, J. W. Kim, Y. S. Lee, J. W. Choi, T. Kang, Y. K. Kim, B. G. Chung, *Nano Convergence* **2021**, *8*, 35.
[4] C. G. Sanchez, F. K. Teixeira, B. Czech, J. B. Preall, A. L. Zamparini, J. R. K. Seifert, C. D. Malone, G. J. Hannon, R. Lehmann, *Cell Stem Cell* **2016**, *18*, 276.
[5] R. Ahrends, A. Ota, K. M. Kovary, T. Kudo, B. O. Park, M. N. Teruel, *Science* **2014**, *344*, 1384.
[6] G. Keller, *Genes Dev.* **2005**, *19*, 1129.
[7] Y. Xu, Y. Shi, S. Ding, *Nature* **2008**, *453*, 338.
[8] A. B. Cherry, G. Q. Daley, *Cell* **2012**, *148*, 1110.
[9] A. P. Chidgey, D. Layton, A. Trounson, R. L. Boyd, *Nature* **2008**, *453*, 330.
[10] Y.-S. Hsiao, Y.-H. Liao, H.-L. Chen, P. Chen, F.-C. Chen, *ACS Appl. Mater. Interfaces* **2016**, *8*, 9275.
[11] F. Pires, Q. Ferreira, C. A. Rodrigues, J. Morgado, F. C. Ferreira, *Biochim. Biophys. Acta, Gen. Subj.* **2015**, *1850*, 1158.
[12] X. Li, S. Y. Tzeng, X. Liu, M. Tammia, Y.-H. Cheng, A. Rolfe, D. Sun, N. Zhang, J. J. Green, X. Wen, *Biomaterials* **2016**, *84*, 157.
[13] B. Shah, P. T. Yin, S. Ghoshal, K. B. Lee, *Angew. Chem., Int. Ed.* **2013**, *52*, 6190.
[14] W. Guo, X. Zhang, X. Yu, S. Wang, J. Qiu, W. Tang, L. Li, H. Liu, Z. L. Wang, *ACS Nano* **2016**, *10*, 5086.
[15] Z. Tang, F. Jiang, Y. Zhang, Y. Zhang, Y. Yang, X. Huang, Y. Wang, D. Zhang, N. Ni, F. Liu, M. Luo, X. Fan, W. Zhang, P. Gu, *Biomaterials* **2019**, *194*, 57.
[16] J. Shao, M. Wang, G. Yu, S. Zhu, Y. Yu, B. C. Heng, J. Wu, H. Ye, *Proc. Natl. Acad. Sci. USA* **2018**, *115*, E6722.
[17] M. R. Love, S. Palee, S. C. Chattipakorn, N. Chattipakorn, *J. Cell. Physiol.* **2018**, *233*, 1860.
[18] L. Braydich-Stolle, S. Hussain, J. J. Schlager, M.-C. Hofmann, *Toxicol. Sci.* **2005**, *88*, 412.
[19] N. Lewinski, V. Colvin, R. Drezek, *Small* **2008**, *4*, 26.
[20] A. Dominguez-Alfaro, N. Alegret, B. Arnaiz, M. Salsamendi, D. Mecerreyes, M. Prato, *ACS Appl. Mater. Interfaces* **2020**, *12*, 57330.
[21] X.-Z. Chen, J.-H. Liu, M. Dong, L. Müller, G. Chatzipirpiridis, C. Hu, A. Terzopoulou, H. Torlakcik, X. Wang, F. Mushtaq, J. Puigmartí-Luis, Q.-D. Shen, B. J. Nelson, S. Pane, *Mater. Horiz.* **2019**, *6*, 1512.
[22] M. Dong, X. Wang, X.-Z. Chen, F. Mushtaq, S. Deng, C. Zhu, H. Torlakcik, A. Terzopoulou, X.-H. Qin, X. Xiao, J. Puigmartí-Luis, H. Choi, A. P. Pêgo, Q.-D. Shen, B. J. Nelson, S. Pané, *Adv. Funct. Mater.* **2020**, *30*, 1910323.
[23] J. H. Lee, H. K. Choi, L. Yang, S. T. D. Chueng, J. W. Choi, K. B. Lee, *Adv. Mater.* **2018**, *30*, 1802762.
[24] X. Wang, S. Li, C. Yan, P. Liu, J. Ding, *Nano Lett.* **2015**, *15*, 1457.
[25] G. H. Altman, R. L. Horan, I. Martin, J. Farhadi, P. R. H. Stark, V. Volloch, J. C. Richmond, G. Vunjak-Novakovic, D. L. Kaplan, *FASEB J.* **2002**, *16*, 1.
[26] J. Fink, M. Théry, A. Azioune, R. Dupont, F. Chatelain, M. Bornens, M. Piel, *Lab Chip* **2007**, *7*, 672.
[27] A. G. Goglia, J. E. Toettcher, *Curr. Opin. Chem. Biol.* **2019**, *48*, 106.
[28] S. Patil, V. Dhyani, T. Kaur, N. Singh, *ACS Appl. Bio Mater.* **2020**, *3*, 3476.
[29] L. R. Polstein, M. Juhas, G. Hanna, N. Bursac, C. A. Gersbach, *ACS Synth. Biol.* **2017**, *6*, 2003.
[30] S. Khan, M. W. Ullah, R. Siddique, G. Nabi, S. Manan, M. Yousaf, H. Hou, *Int. J. Genomics* **2016**, *2016*, 2405954.
[31] T.-H. Kim, C. H. Yea, S. T. D. Chueng, P. T. T. Yin, B. Conley, K. Dardir, Y. Pak, G. Y. Jung, J.-W. Choi, K.-B. Lee, *Adv. Mater.* **2015**, *27*, 6356.
[32] T.-H. Kim, K.-B. Lee, J.-W. Choi, *Biomaterials* **2013**, *34*, 8660.
[33] T.-H. Kim, S. Shah, L. Yang, P. T. Yin, M. K. Hossain, B. Conley, J.-W. Choi, K.-B. Lee, *ACS Nano* **2015**, *9*, 3780.
[34] H. Wang, Y. Li, Y. Zuo, J. Li, S. Ma, L. Cheng, *Biomaterials* **2007**, *28*, 3338.
[35] S. Kang, S. E. Park, D. D. Huh, *Nano Convergence* **2021**, *8*, 20.
[36] H. Ruan, X. Chen, C. Xie, B. Li, M. Ying, Y. Liu, M. Zhang, X. Zhang, C. Zhan, W. Lu, *ACS Appl. Mater. Interfaces* **2017**, *9*, 17745.
[37] W. B. Kauffman, S. Guha, W. C. Wimley, *Nat. Commun.* **2018**, *9*, 2568.
[38] E. S. Ereifej, G. M. Rial, J. K. Hermann, C. S. Smith, S. M. Meade, J. M. Rayyan, K. Chen, H. Feng, J. R. Capadona, *Front. Bioeng. Biotechnol.* **2018**, *6*, 9.
[39] D. Zhou, L. Shao, D. R. Spitz, *Adv. Cancer Res.* **2014**, *122*, 1.
[40] M. P. Lutolf, P. M. Gilbert, H. M. Blau, *Nature* **2009**, *462*, 433.
[41] E. Pazos, P. Novo, C. Peinador, A. E. Kaifer, M. D. García, *Angew. Chem., Int. Ed.* **2019**, *58*, 403.
[42] S. Datta, S. K. Misra, M. L. Saha, N. Lahiri, J. Louie, D. Pan, P. J. Stang, *Proc. Natl. Acad. Sci. USA* **2018**, *115*, 8087.
[43] Q. An, J. Brinkmann, J. Huskens, S. Krabbenborg, J. De Boer, P. Jonkheijm, *Angew. Chem., Int. Ed.* **2012**, *51*, 12233.
[44] Y. M. Zhang, J. H. Liu, Q. Yu, X. Wen, Y. Liu, *Angew. Chem., Int. Ed.* **2019**, *58*, 10553.
[45] S. Sankaran, E. Cavatorta, J. Huskens, P. Jonkheijm, *Langmuir* **2017**, *33*, 8813.
[46] M. Mohammadniaei, T. Lee, J. Yoon, D. Lee, J.-W. Choi, *Biosens. Bioelectron.* **2017**, *98*, 292.
[47] J. Yoon, M. Shin, D. Kim, J. Lim, H.-W. Kim, T. Kang, J.-W. Choi, *Biosens. Bioelectron.* **2022**, *196*, 113725.
[48] R. Shukla, V. Bansal, M. Chaudhary, A. Basu, R. R. Bhonde, M. Sastry, *Langmuir* **2005**, *21*, 10644.
[49] X. Li, L. Wang, Y. Fan, Q. Feng, F.-Z. Cui, *J. Nanomater.* **2012**, *2012*, 6.
[50] Y.-H. Rhee, J. H. Moon, J.-H. Mo, T. Pham, P.-S. Chung, *BMC Cell Biol.* **2018**, *19*, 12.
[51] C. S. von Bartheld, J. Bahney, S. Herculano-Houzel, *J. Comp. Neurol.* **2016**, *524*, 3865.
[52] J. TCW, M. Wang, A. A. Pimenova, K. R. Bowles, B. J. Hartley, E. Lacin, S. I. Machlovi, R. Abdelaal, C. M. Karch, H. Phatnani, P. A. Slesinger, B. Zhang, A. M. Goate, K. J. Brennand, *Stem Cell Rep.* **2017**, *9*, 600.
[53] M. Czepiel, V. Balasubramaniyan, W. Schaafsma, M. Stancic, H. Mikkers, C. Huisman, E. Boddeke, S. Copray, *Glia* **2011**, *59*, 882.

